Science of the Total Environment 544 (2016) 929–938

Contents lists available at ScienceDirect

Science of the Total Environment

journal homepage: www.elsevier.com/locate/scitotenv

A comparison of urban heat islands mapped using skin temperature, air temperature, and apparent temperature (Humidex), for the greater Vancouver area

Hung Chak Ho [a,*], Anders Knudby [b], Yongming Xu [c], Matus Hodul [a], Mehdi Aminipouri [a]

[a] Department of Geography, Simon Fraser University, Burnaby, BC, Canada
[b] Department of Geography, University of Ottawa, Ottawa, ON, Canada
[c] School of Geography and Remote Sensing, Nanjing University of Information Science & Technology, Nanjing, China

HIGHLIGHTS

- Maximum daily apparent temperature (Humidex) is mapped for a complex urban environment
- MODIS, Landsat and DEM data combined to develop regression model
- Spatial Distribution: apparent temperature is broadly similar to that of air temperature, but different from skin temperature
- Some locations are hotspots of apparent temperature, up to 5 degrees above corresponding air temperature

GRAPHICAL ABSTRACT

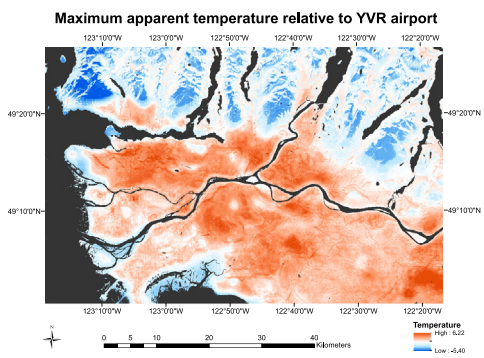

ARTICLE INFO

Article history:
Received 15 November 2015
Received in revised form 1 December 2015
Accepted 4 December 2015
Available online xxxx

Editor: D. Barcelo

Keywords:
Urban heat island
Apparent temperature
Remote sensing
Environmental health
Landsat
MODIS

ABSTRACT

Apparent temperature is more closely related to mortality during extreme heat events than other temperature variables, yet spatial epidemiology studies typically use skin temperature (also known as land surface temperature) to quantify heat exposure because it is relatively easy to map from satellite data. An empirical approach to map apparent temperature at the neighborhood scale, which relies on publicly available weather station observations and spatial data layers combined in a random forest regression model, was demonstrated for greater Vancouver, Canada. Model errors were acceptable (cross-validated RMSE = 2.04 °C) and the resulting map of apparent temperature, calibrated for a typical hot summer day, corresponded well with past temperature research in the area. A comparison with field measurements as well as similar maps of skin temperature and air temperature revealed that skin temperature was poorly correlated with both air temperature ($R^2 = 0.38$) and apparent temperature ($R^2 = 0.39$). While the latter two were more similar ($R^2 = 0.87$), apparent temperature was predicted to exceed air temperature by more than 5 °C in several urban areas as well as around the confluence of the Pitt and Fraser rivers. We conclude that skin temperature is not a suitable proxy for human heat exposure, and that spatial epidemiology studies could benefit from mapping apparent temperature, using an approach similar to the one reported here, to better quantify differences in heat exposure that exist across an urban landscape.

* Corresponding author.
E-mail address: hohungh@sfu.ca (H.C. Ho).

http://dx.doi.org/10.1016/j.scitotenv.2015.12.021
0048-9697/© 2015 Published by Elsevier B.V.

1. Introduction

Extreme heat events regularly lead to excess mortality, as documented from the United States (Curriero et al., 2002; Kaiser et al., 2001; Medina-Ramón et al., 2006; Semenza et al., 1996), Europe (Filleul et al., 2006; Schifano et al., 2009), China (Huang et al., 2010), Russia (Trenberth and Fasullo, 2012), and Canada, where heat-caused excess mortality has been documented for Vancouver (Kosatsky et al., 2012), Montreal (Smargiassi et al., 2009), and Toronto (Pengelly et al., 2007). Elevated temperature can also increase the severity of air pollution, thus compounding human health risks (Katsouyanni et al., 1993; Koken et al., 2003) and leading to increases in hospitalization rates (Koken et al., 2003; Schwartz et al., 2004).

Appropriate quantification of human heat exposure is a necessary foundation for studying the effect of heat on human health. While there is a wealth of research on thermal indices related to human thermal comfort (e.g. Höppe, 1999; Matzarakis et al., 1999), epidemiological studies of extreme heat events and their health impacts typically quantify a population's heat exposure as the near-surface air temperature reported from a local reference station (e.g. the local airport), most often using daily or two-day averaged minimum or maximum air temperatures (Basu, 2009; Hajat et al., 2010; Kosatsky et al., 2012; Smargiassi et al., 2009). While the use of a single reference station is straightforward, easy to understand, and ensures consistency through time, it also ignores well-known differences in temperature that typically exist between different parts of an urban area (Ghosh and Joshi, 2014; Maimaitiyiming et al., 2014; Nichol and To, 2012; Rajasekar and Weng, 2009; Wu et al., 2013; Zhou et al., 2012), and between urban and rural areas (an effect known as the urban heat island), and it thus ignores what are often substantial differences in heat exposure between populations living in different parts of the area in question (Basu, 2009).

Attempts to incorporate local temperature variability in heat–health studies have typically relied on satellite-derived estimates of skin temperature, also known as "land surface temperature" (Buscail et al., 2012; Hondula et al., 2012; Laaidi et al., 2012; Smargiassi et al., 2009; Tomlinson et al., 2011).While results are occasionally ambiguous concerning the importance of this variable in determining health risk (INVS, 2004), several such studies have demonstrated that living in a relatively hot part of a city is a significant risk factor during extreme heat events (Laaidi et al., 2012; Smargiassi et al., 2009). However, the use of skin temperature to quantify heat exposure in these studies seems primarily motivated by the relative ease with which this variable can be mapped, and not by considerations concerning its conceptual appropriateness as a proxy for human heat exposure. Skin temperature is relatively straight-forward to map from publicly available satellite data (Coll et al., 2010; Weng et al., 2004) because the longwave thermal radiation measured by the satellite sensor is strongly determined by the skin temperature under normal atmospheric conditions. However, it can only be mapped at the time of satellite overpass. For the Landsat sensors typically used to obtain neighborhood-level spatial resolution, this means that the resulting maps describe the distribution of skin temperature at approximately 10 am local time. SEVIRI, AVHRR, MODIS and other sensors less frequently used in spatial epidemiology can provide information multiple times per day, but do so at much reduced spatial resolution.

Potential alternative measures of heat exposure that are practical for public health research include air temperature or apparent temperature, a measure of the ambient heat perceived by humans that is typically calculated using both air temperature and humidity (Basu, 2009; Massetti et al., 2014; Steadman, 1979). Either of these can be quantified as the daily minimum, mean, maximum, or as multi-day average values of these quantities. Both air temperature and apparent temperature are more frequently used than skin temperature to quantify heat exposure in the non-spatial epidemiology literature, but they are also more difficult to map at the urban/neighborhood scale. Mapping air temperature requires spatial interpolation between a dense network of weather stations (Hattis et al., 2012), statistical approaches based on the presence of very dense vegetation in the local area (Prihodko and Goward, 1997; Zakšek and Schroedter-Homscheidt, 2009) or regression modeling with local calibration data (Ho et al., 2014; Nichol and To, 2012; Xu et al., 2014). Uneven distribution of weather stations in most urban areas, and especially the lack of observations in densely built-up areas where the urban heat island effect is strongest, are serious shortcomings for the interpolation approach, and the presence of very dense vegetation cannot be assumed in all urban areas. The regression approach, however, has been shown effective for mapping intra-urban variation in air temperature, and application to apparent temperature is straight forward.

While energy fluxes ensure a relationship between the skin temperature and the temperature and humidity of the air mass above it, the relationship between skin, air, and apparent temperature is complex as each temperature measure is also influenced by other factors such as wind speed and direction, the three-dimensional structure of the surface and its effect on both shading and turbulence, the land surface heat capacity, and near-surface water available for evapotranspiration. It is therefore not evident that the spatial pattern of one (e.g. skin temperature) is a good proxy for another (e.g. air temperature), nor that mapping mid-morning skin temperature, as is typically done using Landsat data, is the best approach to quantify human heat exposure in different parts of a city. While apparent temperature is often highly correlated with air temperature, it has been shown to be more closely related to mortality than other temperature variables (Almeida et al., 2010, Barnett et al., 2010, Zhang et al., 2014), and has also been shown to be a better predictor of indoor temperature than is air temperature (Nguyen et al., 2014). As a proxy for heat exposure this is especially important given that people in most industrialized countries spend >90% of their time indoors (Höppe and Martinac, 1998). It is therefore likely that maps of apparent temperature would be a good source of information on heat exposure in heat health studies.

To investigate how the three heat exposure measures are spatially distributed and hence how the choice of heat exposure measure will influence its quantification in heat health studies, building on previous work (Ho et al., 2014), we 1) test the accuracy with which the fine-scale distribution of apparent temperature can be mapped in the greater Vancouver area, and 2) compare the spatial distribution of skin temperature, air temperature, and apparent temperature for hot summer days in the area. The mapping approach from this study can also be used to estimate the spatial distributions of apparent temperature for the long-term risk assessment, by combining scenes of satellite images from different year to map the heat exposure in a typical hot summer day.

2. Study area

The greater Vancouver area, Canada (Fig. 1), is a metropolitan area with a population of more than 2 million (Statistics Canada, 2007). The area is bordered by fold mountain ridges to the north, the Pacific Ocean to the west, and the semi-arid Fraser Valley to the east, a geographic context that creates a complex microclimate system in the area (Oke, 1976; Oke and Hay, 1994; Runnalls and Oke, 2000). On a typical hot summer day, with cloudless skies and light winds from the Fraser Valley the previous night, a strong urban heat island effect can develop in the area, substantially elevating the temperature in the urban areas relative to their surroundings (Oke and Hay, 1994).

3. Data and methods

3.1. Humidex field observations

Maximum air temperature and dew point data were obtained from 39 weather stations operated by Environment Canada or the Weather Underground; the latter is a volunteered geographic information

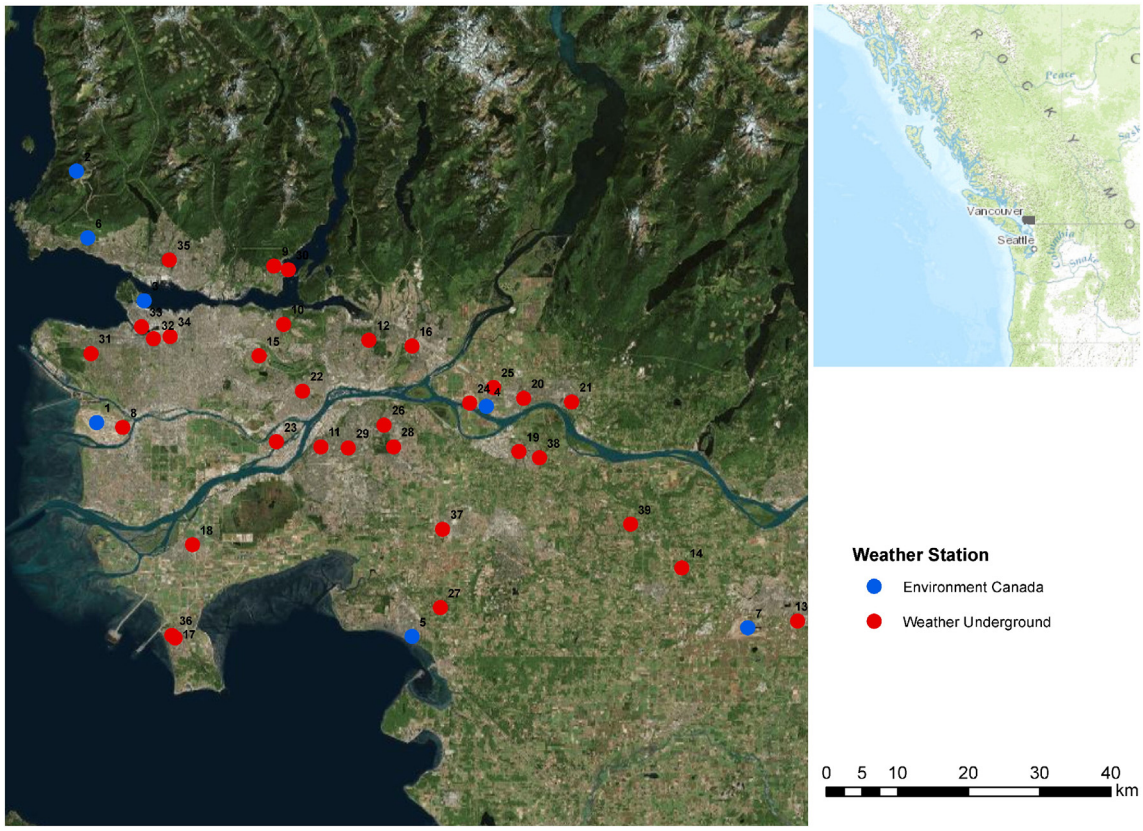

Fig. 1. The greater Vancouver area. The blue points are weather stations from Environment Canada and red points are weather stations from the Weather Underground, from which temperature and humidity observations were used to calibrate the regression model. (For interpretation of the references to color in this figure legend, the reader is referred to the web version of this article.)

program in which participants deploy personal weather stations and upload weather data to an open-access web GIS (Goodchild, 2007; Sieber, 2006). Data were obtained for all (six) hot summer days in the period 2002–2009 for which cloud-free Landsat satellite images were also available (Table 1), all with a maximum air temperature higher than 25 °C at the Vancouver International Airport (YVR). Using only data from hot summer days ensured that the results are calibrated to such days, when the risk of heat-caused human health problems is greatest. Not every weather station was operational for all six days used in this study; several Weather Underground and Environment Canada stations only had data available for one or two days of the six days. For each observation, maximum air temperature and co-incident dew point data were used to calculate apparent temperature using the Humidex, a well-known heat index used to quantify heat exposure in Canada (Burke et al., 2006; Gosling et al., 2014; Masterson and Richardson, 1979). The Humidex is defined as:

$$H = Ta + 0.5555 \times \left(6.11 \times e^{5417.753 \times \left(\frac{1}{273.16} - \frac{1}{dew}\right)} - 10\right)$$

Table 1
Landsat images used for this study. The images were obtained for cloud-free hot summer days in the study area.

Satellite images	Acquired date	Daily maximum air temperature at Vancouver International Airport
Landsat 5 TM	13/08/2002	27.1
Landsat 5 TM	17/07/2004	27.1
Landsat 7 ETM+	02/08/2004	25.4
Landsat 5 TM	23/07/2006	26.7
Landsat 5 TM	12/07/2008	25.5
Landsat 7 ETM+	31/07/2009	28.7

where H is the Humidex, Ta is the air temperature, and dew is the dew point in Kelvin.

3.2. Spatial data layers

Spatial data layers containing potential predictors of apparent temperature for use in regression modeling were derived from four different sources. 1) Cloud-free Landsat 5 TM and Landsat 7 ETM+ images were obtained for the six days for which field observations were available, and 2) a land surface emissivity data set was retrieved from the North American ASTER Land Surface Emissivity Database (NAALSED) (Hulley and Hook, 2009). In addition, 3) a Digital Elevation Model (DEM) was obtained from the 25-m Canadian Digital Elevation Data (CDED, http://www.geobase.ca), and 4) the MODIS Precipitable Water product (MOD05) was used to provide information on atmospheric water vapor content for the six days with Landsat data.

The Landsat 5 TM images, the MODIS water vapor product and the DEM were all resampled to 60-m cell sizes to match the spatial resolution of the ETM+ thermal band, and all data were re-projected to the Universal Transverse Mercator projection, Zone 10 N. Areas affected by Scan-Line Corrector (SLC) errors in each Landsat ETM+ image were masked out prior to further analysis.

3.3. Regression modeling

The following environmental data layers were derived from the satellite and digital elevation data and used as predictors of apparent temperature in a regression model: 1)skin temperature (LST), 2) elevation, 3) the Normalized Difference Water Index (NDWI), 4) SkyView Factor (SVF), 5) incident solar radiation, 6) distance from the ocean, and 7) atmospheric water vapor.

LST was estimated from the thermal band in the Landsat images. NASA's Atmospheric Correction Parameter Calculator (Barsi et al., 2003) was used to estimate the upwelling atmospheric radiance ($L^{\uparrow}$), downwelling atmospheric radiance ($L^{\downarrow}$) and atmospheric transmittance τ, which were then used with the NAALSED emissivity values (ε) to obtain the blackbody radiance at temperature LST:

$$B(LST) = \frac{L_{sen} - L^{\uparrow}}{\varepsilon\tau} - \frac{1-\varepsilon}{\varepsilon} L^{\downarrow} \text{(Coll et al., 2010)}$$

where B(LST) is the blackbody radiance at temperature LST and L_{sen} is the at-sensor radiance. An inversion of Planck's Law was then applied to derive the kinetic skin temperature using the following equation:

$$LST = \frac{k_2}{\ln\left(\frac{k_1}{B(LST)} + 1\right)}$$

where k_1 and k_2 are the thermal band calibration constants found in the Landsat metadata files.

NDWI is an index used to quantify water content in vegetation cover (Gao, 1996), which strongly influences evapotranspiration and thus cooling of the land surface during a hot day. NDWI is defined as:

$$NDWI = (\rho_{NIR} - \rho_{MIR})/(\rho_{NIR} - \rho_{MIR})$$

where ρ_{NIR} is surface reflectance in the near-infrared band, and ρ_{MIR} is surface reflectance in the mid-infrared band. Landsat bands 4 and 5 were used to calculate NDWI. NDWI is not meaningful for water bodies; to ensure its use as a proxy for evapotranspiration we therefore applied the maximum NDWI value found over land to all pixels identified as water.

SVF quantifies the unobscured portion of the sky, is determined by topography and the presence of above-ground structures such as trees and buildings, and influences the radiation received and emitted from a surface (Chen et al., 2012; Su et al., 2008; Yang et al., 2015). Fenner et al. (2014) found that relatively low SVF in an urban area dampens diurnal air temperature variations, with a cooling effect during the day and a warming effect during the night. SVF was derived for each cell using a two-step process, initially using partial spectral unmixing to derive an estimate of the shadow proportion of the cell, then using an empirically calibrated regression model to derive SVF from the shadow proportion. Full details of this method will be forthcoming in a separate paper, validation using airborne lidar data from the City of Vancouver indicate good performance (SVF RMSE = 0.056).

Incident solar radiation influences skin temperature, and hence air temperature (Bristow and Campbell, 1984). Using the DEM, the direct solar radiation tool in ArcGIS 10.1 was applied to estimate the incoming solar radiation for each cell (Fu and Rich, 2002). This tool estimates the total direct solar radiation from all sun map sectors:

$$Solar\ Radiation = S_{Const}\beta^{m(\theta)} \times SunDur_{\theta,\alpha} \times SunGap_{\theta,\alpha} \times \cos(AngIn_{\theta,\alpha})$$

where S_{Const} = solar flux, β = atmospheric transmittance, $m(\theta)$ = optical path length, $SunDur_{\theta,\alpha}$ = time duration represented by the sky sector, $SunGap_{\theta,\alpha}$ = the gap fraction for the sun map sector, $AngIn_{\theta,\alpha}$ = the angle of incidence, and θ = the solar zenith angle.

Distance from the ocean was estimated from the Vegetation Resources Inventory (VRI) land cover map by Ministry of B.C (Taylor, 1998). All terrestrial land cover classes were joined to create a binary classification with only “water” and “land” categories from which the distance to the ocean was calculated.

Atmospheric water vapor was derived from the MODIS Precipitable Water product (MOD05)near-infrared total-column precipitable water, which is known to be sensitive to near-surface water vapor in the canopy layer (King et al., 2003; Wong et al., 2014). The canopy layer is the layer within 2 m above the land surface, which is a key component of urban heat island and the atmospheric layer most important to environmental health studies (Oke, 1976).

Spatial averaging was applied to the LST and NDWI layers to account for the influence of these surface variables in areas around each weather station (Liu and Moore, 1998; Zakšek and Oštir, 2012). A range of circular kernels were tested for this spatial averaging, with radii ranging from 100 m to 1000 m in 100-m intervals. To determine which LST kernel radius would lead to the best model performance, spatially averaged LST data layers were included individually in the model in combination with all other data layers, and cross-validation used to quantify model performance. The LST kernel radius that achieved the lowest RMSE value was retained. A similar process was performed to determine the best NDWI kernel radius. In subsequent model runs, only the best spatially averaged LST and NDWI data layers in combination with all other data layers were used as predictors of apparent temperature.

A random forest regression model was used to formalize the relationship between these spatial data layers and the apparent temperature data. Random forest is a non-parametric machine learning model that uses an ensemble of regression trees, each trained on a random subset of the training data, with a random subset of the available predictors used to split the data in each node of each tree (Breiman, 2001; Stumpf and Kerle, 2011; Timm and McGraigal, 2012). We used the randomForest package (Liaw and Wiener, 2012) in the statistical software R, with default parameter settings (Hijmans and van Etten, 2009; Liaw and Wiener, 2012; Meyer et al., 2012; R Core Development Team, 2008), which had previously proven effective at similarly mapping air temperature (Ho et al., 2014). The model was first used to predict the maximum apparent temperature for each of the six days for which we had satellite data (Table 1), and the value predicted for YVR was then subtracted to produce a relative temperature measure. The mean of these predictions of maximum apparent temperature relative to YVR was then calculated to represent the relative apparent temperature on a typical hot summer day.

3.4. Accuracy assessment

The random forest model was validated using leave-one-station-out cross validation to provide an estimate of prediction errors in unsampled areas. In this procedure apparent temperature observations from a single station were held aside while observations from all other weather stations were used to train the regression model, and predictions were then compared to observations for the held-out station to determine the prediction error. This process was repeated until observations from each station were used for validation once, and the Mean Average Error (MAE) and Root Mean Square Error (RMSE) averaged across all stations reported (Willmott and Matsuura, 2005). Cross-validation is a well-known method for accuracy assessment, and is commonly used to validate machine learning models (Gislason et al., 2006; Zhang, 1993).

3.5. Variance importance analysis

The permutation-based variance importance analysis implemented in the randomForest package was used to determine the contributions of each predictor to the regression model (Genuer et al., 2010; Knudby et al., 2010; Strobl et al., 2009). For each regression tree, the data that were not used to ‘grow’ the tree were initially used to assess prediction error. For these data points, each predictor was then permuted in turn and the resulting increase in prediction error recorded. This was done for all trees, and the average reported as the percentage increase in mean squared error (%IncMSE).

3.6. Production of temperature maps

The random forest model was applied to the spatial data layers to produce maps of the distribution of maximum apparent temperature in the study area, relative to YVR, for the six days studied. The maps produced with the four Landsat 5 TM images were then averaged to produce a single map representative of a typical hot summer day in the area; Landsat 7 ETM+ images were not used for this averaging due to the SLC errors. An identical approach to the one described above, but using maximum air temperature instead of maximum apparent temperature as the dependent variable in the random forest model, was used to produce a comparable map of maximum air temperature. In addition, a skin temperature map was created by calculating the mean of the LST values derived from each of the four Landsat 5 TM images.

4. Results

4.1. Predictions of apparent temperature

In general, larger radii used for spatial averaging resulted in lower prediction errors for apparent temperature. LST averaged over the largest radii (1000 m) produced the lowest prediction error, as did NDWI averaged over 500 m. Using this spatially averaged LST and NDWI layers along with the other predictors, the MAE and RMSE values from the random forest model were 1.67 °C and 2.04 °C respectively ($R^2 = 0.57$; Fig. 2), which is relatively accurate compared to similar air temperature mapping studies (Benali et al., 2012; Ho et al., 2014; Prihodko and Goward, 1997; Zakšek and Schroedter-Homscheidt, 2009). Very high values of apparent temperature were typically underestimated, and one low value was significantly overestimated. This is a known issue caused by the random forest model structure, in which predictions are not extrapolated beyond the values included in the training data. The issue may have been further affected by the presence of important predictors not included in the model, such as wind speed and anthropogenic heat generation (Oke, 1988). Similar results were seen for predictions of air temperature, with MAE and RMSE values of 1.50 °C and 1.90 °C respectively, and was also fairly accurate compared to other air temperature mapping studies (Benali et al., 2012; Ho et al. 2014; Prihodko and Goward, 1997; Zakšek and Schroedter-Homscheidt, 2009).

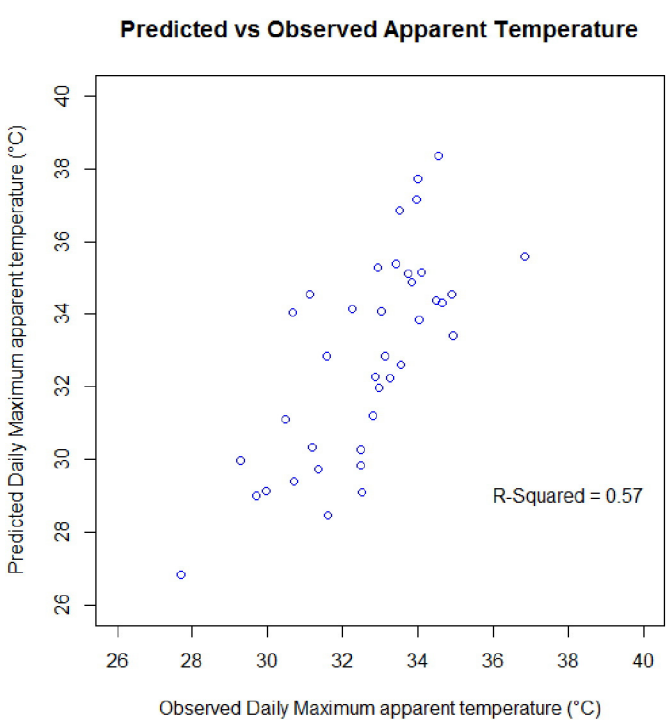

Fig. 2. Scatterplot of predicted vs. observed maximum apparent temperature.

4.2. Variable importance

The variable importance results for all predictors are shown in Table 2. The most important predictor was LST, which is known to directly influence air temperature through radiative, conductive, and convective heat transfer (Bristow and Campbell, 1984; Vancutsem et al., 2010). Atmospheric water vapor and distance from the ocean also had high variable importance scores, which was expected as one directly quantifies humidity and the other influences the strength of the moderating influence of the ocean. SVF had only moderate variable importance, however, given that no weather stations were located in very low SVF areas such as downtown Vancouver, the actual influence of SVF on apparent temperature in such areas is not captured in the model and the importance of SVF across the study area may thus be underestimated. A similar effect may have caused the low variable importance values of the NDWI and elevation predictors, as only a few weather stations are located in high NDWI (forest) and high elevation (mountain) locations.

4.3. Spatial distribution of the three temperature measures

Maps showing the distribution of each temperature measure on a typical hot summer day in the study area are shown in Fig. 3. The distribution of maximum apparent temperature (Fig. 3c) corresponds well with past temperature research in the greater Vancouver area (Oke and Hay, 1994), and showed that relatively high apparent temperatures are found in urban areas, while low apparent temperatures are found in the mountainous areas of West and North Vancouver. Agricultural lands and forests were predicted as relatively cool, and downtown Vancouver was predicted to be relatively cooler than other major urban areas. This latter result is likely due to a sea breeze cooling the downtown core, which is surrounded by water to the south, west, and northeast(Runnalls and Oke, 2000). A "wall effect" (Wong et al., 2011)in which cold air is trapped within the urban canyon at night and the early morning, reducing air flow and preventing direct solar radiation from increasing the temperature of the downtown air mass during the day, could also be a contributing factor.

The spatial temperature trends are broadly similar between the three temperature measures, with urban areas being relatively warm while forested and mountainous areas are relatively cool, however, notable differences also exist.LST values (Fig. 3a) in the area range from almost 50 degrees cooler to almost 15 degrees warmer than YVR, while air temperature and apparent temperature values have a smaller value range. In addition, the LST map shows strong contrasts in temperature between adjacent areas, while values vary more gradually in the air temperature (Fig. 3b) and apparent temperature (Fig. 3c) maps. This difference in local contrast is partly a result of data layers with low local contrast having been used to produce the air temperature and apparent temperature maps, notably the spatially averaged LST and NDWI

Table 2
Results from the variable importance analysis. The percentage increase in mean squared error (%IncMSE) quantifies the increase in prediction error caused by the permutation of each individual predictor in the validation data.

Variable	%IncMSE
LST (1000 m)	26.68
Atmospheric water vapor	17.65
Distance from ocean	14.81
SVF	9.01
Solar radiation	5.81
NDWI (500 m)	2.84
Elevation	1.92

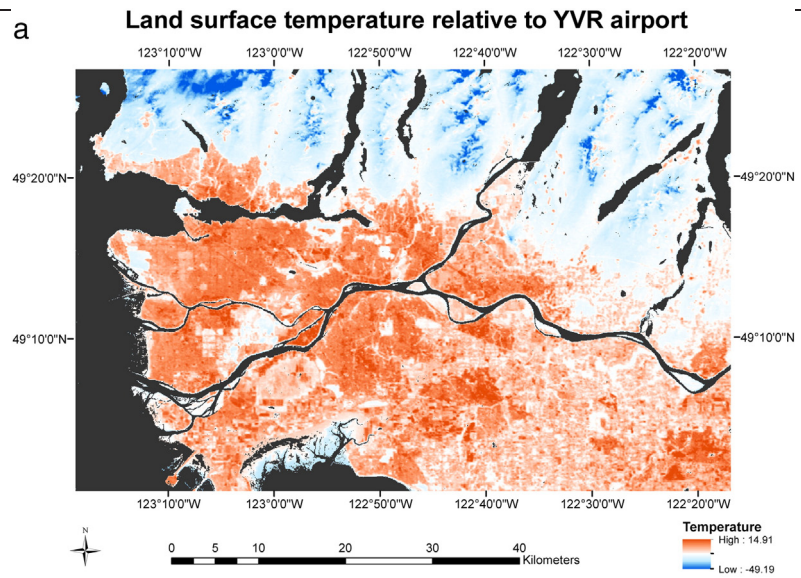
a
Land surface temperature relative to YVR airport
123°10'0"W
123°0'0"W
122°50'0"W
122°40'0"W
122°30'0"W
122°20'0"W
49°20'0"N
49°10'0"N
0 5 10 20 30 40
Kilometers
Temperature
High : 14.91
Low : -49.19

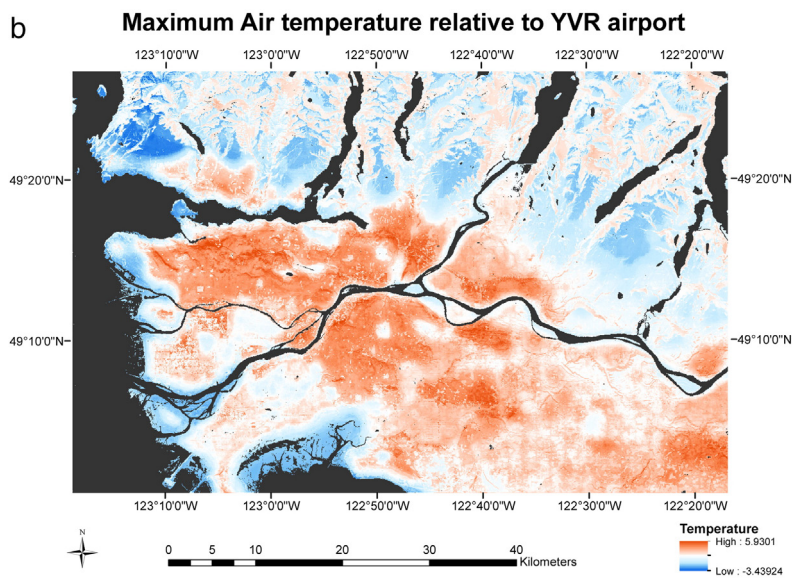
b
Maximum Air temperature relative to YVR airport
123°10'0"W
123°0'0"W
122°50'0"W
122°40'0"W
122°30'0"W
122°20'0"W
49°20'0"N
49°10'0"N
0 5 10 20 30 40
Kilometers
Temperature
High : 5.9301
Low : -3.43924

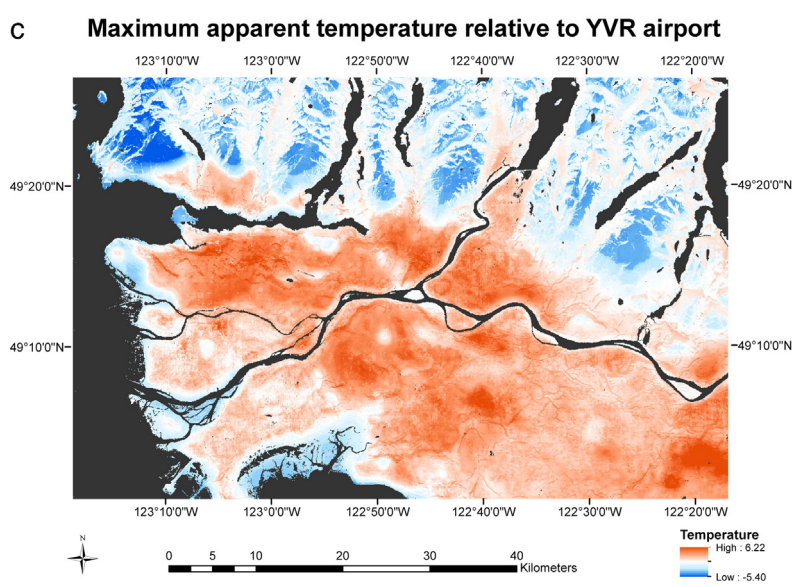
c
Maximum apparent temperature relative to YVR airport
123°10'0"W
123°0'0"W
122°50'0"W
122°40'0"W
122°30'0"W
122°20'0"W
49°20'0"N
49°10'0"N
0 5 10 20 30 40
Kilometers
Temperature
High : 6.22
Low : -5.40

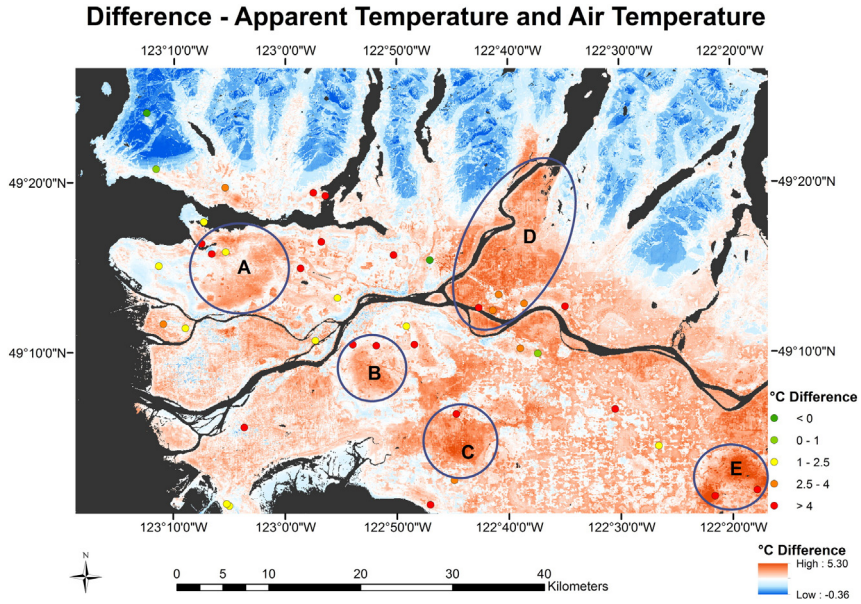

Fig. 4. Predicted apparent temperature minus air temperature for a typical hot summer day in the greater Vancouver area. Circles indicate hot spots of apparent temperature. Top left (circle A): Central Burnaby and East Vancouver. Bottom left: Central Surrey (circle B) and Cloverdale (circle C). Top right (circle D): Pitt Meadows and Port Coquitlam at the confluence of the Pitt and Fraser Rivers. Bottom right (circle E): Abbotsford. Points indicate average differences between apparent and air temperatures observed at weather stations on hot summer days.

data layers as well as the 'distance from the ocean' layer. However, it is also a realistic description of LST being strongly dependent on the radiative and thermal properties of the surface material while air temperature and apparent temperature are relatively more influenced by advection and thus by surface conditions in a larger upwind area (Stewart and Oke, 2012). The LST distribution is poorly correlated to both that of air temperature ($R^2 = 0.38$) and apparent temperature ($R^2 = 0.39$), a result that is confirmed by correlations between the weather station observations themselves ($R^2 = 0.15$ and $R^2 = 0.11$, respectively). While the air temperature and apparent temperature distributions show much greater similarity (R^2 of model outputs $= 0.87$; R^2 of weather station data $= 0.74$), several areas of interest are predicted to have relatively high apparent temperatures, indicating high humidity and thus high Humidex values on hot summer days. Some of these areas are highlighted with blue circles in Fig. 4, which shows the difference between the predicted apparent and air temperatures. Hot spots of apparent temperature, relative to air temperature, include some of the densely built-up neighborhoods in East Vancouver and central Burnaby, downtown Surrey, the small community of Cloverdale, the confluence of the Pitt and Fraser rivers, and the city of Abbotsford. In these areas, predicted apparent temperatures are up to 5 degrees higher than the corresponding air temperatures.

5. Discussion

5.1. Apparent temperature patterns and variability

A critical assumption when mapping temperature distributions for a 'typical' hot summer day is that weather and temperature patterns are similar between hot summer days, and that the mapped temperature distribution is therefore a meaningful representation of conditions on a 'typical' hot summer day. A typical weather pattern has indeed been shown to exist for hot summer days in the area, with positive anomalies of the 500-hPa geopotential heights and 850-hPa temperatures centered over the British Columbia coast, and negative anomalies of sea level pressure centered off the coast of Washington State (Bumbaco et al., 2013), leading to cloudless skies and light winds from the Fraser Valley (Oke and Hay, 1994). Nevertheless, Fig. 5 indicates that some variation exists in daily maximum apparent temperature, relative to YVR, observed at each weather station on the days used in our study. While several weather stations (e.g. stations 5, 16, 17, 18, 27) show variations in temperature that include values both higher and lower than YVR, other stations are either consistently warmer than YVR for the days included in the study (e.g. station 13), or consistently colder (e.g. station 2).

Closer examination of each station's local landscape context showed that stations with high apparent temperatures relative to YVR were typically found near sparsely built-up or agricultural areas, as were the case for Abbotsford and Pitt Meadows respectively. Stations with relatively low apparent temperatures were found in the forested and mountainous areas in the northern part of the study area. Stations with high temperature variability were primarily found in suburban areas near the coast, a context that allows wind speed and direction great influence on the local temperature (Runnalls and Oke, 2000).

Apart from the local landscape context, imperfect data quality may also have contributed to the observed temperature variability. Many Environment Canada weather stations only provide records of temperature and dew point in the form of daily minima and maxima, which are not suitable for calculation of maximum apparent temperature because the maximum temperature and the maximum dew point may not occur at the same time. As a result, data from these stations could not be used in this study. Weather Underground stations typically provide hourly values of the same measurements, as a result 82% of the weather stations used in this study belonged to the Weather Underground. Environment Canada follows guidelines from the World Meteorological Organization (WMO) when deploying weather stations, which ensures that these are located away from large buildings, reflective surfaces, and other sources of heat or radiation (World Meteorological Organization, 2008). While this aims to ensure that measurements are representative of the air mass in the surrounding area, it also precludes deployment of weather stations in the urban areas which are of greatest interest from a human health perspective. Weather Underground provides similar guidelines for deployment of weather stations, but does not control that these guidelines are followed by the volunteers contributing to its

Fig. 3. Spatial distribution of LST (Fig. 3a — top), air temperature (Fig. 3b — middle), and apparent temperature (Fig. 3c — bottom) in the greater Vancouver area for a typical hot summer day. Waterbodies are masked out (black). All values are normalized to YVR.

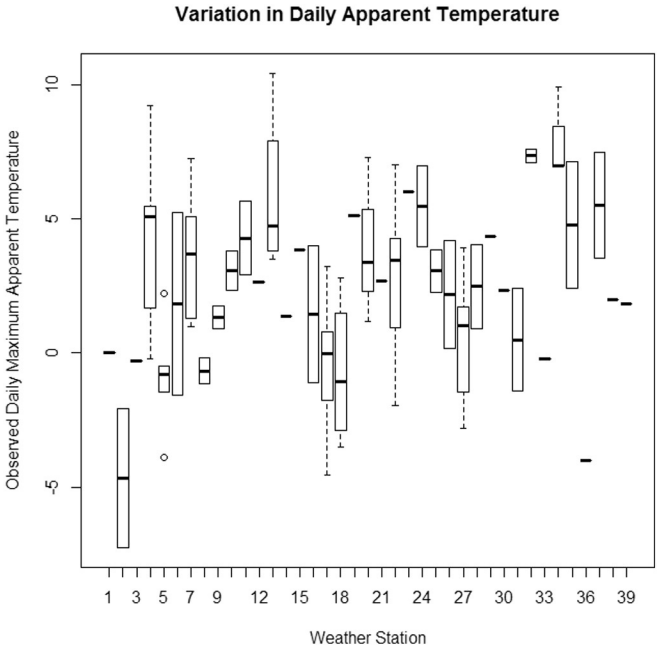

Fig. 5. Variation of observed daily maximum apparent temperatures, relative to YVR, for each weather station. Boxes indicate the interquartile range as well as the median (bold line), whiskers extend to the most extreme data point which is no more than 1.5 times the interquartile range from the box, and circles indicate more extreme data points. For stations with only a single observation only that (median) value is shown.

database, nor does it control the quality of the resulting data. In fact, some Weather Underground stations located in heavily urbanized areas do not conform to WMO guidelines. In this study the two data sources were combined to improve coverage of the different local landscape contexts found in the area. However, the lack of quality control may have resulted in some Weather Underground stations being improperly placed or operated, which may have introduced a positive bias in apparent temperature measurements for urban areas that, in our study, which are only covered by Weather Underground stations. The importance of quality control for Weather Underground data, and for volunteered geographic information (VGI) more broadly, will increase in the future as the volume of VGI data increases. An alternative to VGI for generating temperature data in urban areas is mobile temperature measurements, which allows user-defined quality control but also requires additional resources for data collection (Anderson and Bell, 2011).

5.2. Comparison and validation of temperature distributions

Despite the strong correlation between the predicted air temperature and apparent temperature, important differences exist in their spatial distribution, especially in the areas circled in Fig. 4 where apparent temperatures typically exceed air temperatures by up to 5 °C. Several urban centers show relatively large differences between apparent temperature and air temperature, including Abbotsford, Cloverdale, Surrey, and parts of Burnaby and Vancouver. While this is an intriguing result and weather station data confirm the existence of such differences in the study area, no weather stations whose observations could validate the result are located in the cores of these areas. However, coverage of weather stations in the Weather Underground network is rapidly expanding in the study area and it is hoped that this particular result can be validated with field observations in the near future. On the other hand, several weather stations are located near the confluence of the Pitt and Fraser rivers, confirming that this area experiences relatively high apparent temperatures. Given that many large cities are located in river valleys, on deltas, or on historical floodplains (e.g. New York City, Hong Kong, London, and Shanghai), the relatively high apparent temperatures observed in both urbanized areas and at the confluence of the two rivers has important implications for mapping human heat exposure in urban areas and their surroundings. The differences in the spatial distributions of all three temperature measures are especially important because apparent temperature has been shown to be the most closely linked to urban heat health, indoor temperature (Nguyen et al., 2014), and mortality during extreme heat events (Almeida et al., 2010; Barnett et al., 2010; Zhang et al., 2014). It is likely that heat-related spatial epidemiology studies will benefit from using apparent temperature instead of LST to quantify human heat exposure.

6. Conclusion

Weather station observations and spatial data layers derived from satellite imagery and a digital elevation model were combined in a random forest regression model to produce predictions of the daily maximum apparent temperature for unsampled areas (cross-validated RMSE = 2.04 °C). Predictions were normalized to values at Vancouver International Airport, and the model was applied to the spatial data layers to produce a map of relative daily maximum apparent temperature for a typical hot summer day in the greater Vancouver area, Canada. Comparable maps were produced for daily maximum air temperature and mid-morning skin temperature. Skin temperature was poorly correlated with the two other temperature measures ($R^2 = 0.38$ and 0.39 respectively). While air temperature and apparent temperature showed greater similarity ($R^2 = 0.87$), the apparent temperature exceeded the air temperature by more than 5 °C in several urban areas as well as around the confluence of the Pitt and Fraser rivers. Skin temperature is not a suitable proxy for human heat exposure, and spatial epidemiology studies could benefit from mapping apparent temperature, using an approach similar to the one reported above, to better quantify differences heat exposure that exist across an urban landscape.

Acknowledgments

The authors acknowledge the Pacific Institute for Climate Solutions and Simon Fraser University for providing full support and partial funding for this project. We also acknowledge Dr. Sarah B. Henderson from the British Columbia Centre for Disease Control for her many contributions to this work, and Paul Sirovyak from Simon Fraser University for data processing support.

References

Almeida, S.P., Casimiro, E., Calheiros, J., 2010. Effects of apparent temperature on daily mortality in Lisbon and Oporto, Portugal. Environ. Heal. 9 (1), 12.
Anderson, G., Bell, M., 2011. Heat waves in the United States: mortality risk during heat waves and effect modification by heat wave characteristics in 43 U.S. communities. Environ. Health Perspect. 119 (2), 210–218.
Barnett, A.G., Tong, S., Clements, A.C.A., 2010. What measure of temperature is the best predictor of mortality? Environ. Res. 110 (6), 604–611.
Barsi, J.A., Barker, J.L., Schott, J.R., 2003. An atmospheric correction parameter calculator for a single thermal band earth-sensing instrument. Toulouse, France: IGARSS IEEE International Geoscience and Remote Sensing Symposium.
Basu, R., 2009. High ambient temperature and mortality: a review of epidemiologic studies from 2001 to 2008. Environ. Heal. 8 (1), 40.
Benali, A., Carvalho, A., Nunes, J., Carvalhais, N., Santos, A., 2012. Estimating air surface temperature in Portugal using MODIS LST data. Remote Sens. Environ. 124 (2012), 108–121.
Breiman, L., 2001. Random forests. Mach. Learn. 45 (1), 5–32.
Bristow, K., Campbell, G., 1984. On the relationship between incoming solar radiation and daily maximum and minimum temperature. Agric. For. Meteorol. 31, 159–166.
Bumbaco, K.A., Dello, K.D., Bond, N.A., 2013. History of Pacific Northwest heat waves: synoptic pattern and trends. J. Appl. Meteorol. Climatol. 52, 1618–1631.
Burke, M., Sipe, N., Evans, R., Mellifont, D., 2006. Climate, geography and the propensity to walk: environmental factors and walking trip rates in Brisbane. Papers of the 29th Australasian Transport Research Forum, Gold Coast, 27–29 September 2006.
Buscail, C., Upegui, E., Viel, J.-F., 2012. Mapping heatwave health risk at the community level for public health action. Int. J. Health Geogr. 11, 38.
Chen, L., Ng, E., An, X., Ren, C., Lee, M., Wang, U., He, Z., 2012. Sky view factor analysis of street canyons and its implications for daytime intra-urban air temperature differentials in high-rise, high-density urban areas of Hong Kong: a GIS-based simulation approach. Int. J. Climatol. 32, 121–136.

Coll, C., Galve, J.M., Sánchez, J.M., Caselles, V., 2010. Validation of Landsat-7/ETM + thermal-band calibration and atmospheric corrections with ground based measurements. IEEE Trans. Geosci. Remote Sens. 48 (1), 547–555.

Curriero, F.C., Heiner, K.S., Samet, J.M., Zeger, S.L., Strug, L., Patz, J.A., 2002. Temperature and mortality in 11 cities of the eastern United States. Am. J. Epidemiol. 155 (1), 80–87.

Fenner, D., Meier, F., Scheret, D., Polze, 2014. Spatial and temporal air temperature variability in Berlin, Germany, during the years 2001–2010. Urban Climate 10, 308–331.

Filleul, L., Cassadou, S., Médina, S., Fabres, P., Lefranc, A., Eilstein, D., ... Ledrans, M., 2006. The relation between temperature, ozone, and mortality in nine French cities during the heat wave of 2003. Environ. Health Perspect. 114 (9), 1344–1347.

Fu, P., Rich, P., 2002. A geometric solar radiation model with applications in agriculture and forestry. Comput. Electron. Agric. 37, 25–35.

Gao, B.-C., 1996. NDWI—a normalized difference water index for remote sensing of vegetation liquid water from space. Remote Sens. Environ. 58, 257–266.

Genuer, R., Poggi, J.-M., Tuleau-Malot, C., 2010. Variable selection using random forests. Pattern Recogn. Lett. 31 (14), 2225–2236.

Ghosh, A., Joshi, P.K., 2014. Hyperspectral imagery for disaggregation of land surface temperature with selected regression algorithms over different land use land cover scenes. ISPRS J. Photogramm. Remote Sens. 96, 76–93.

Gislason, P., Benediktsson, J., Sveinsson, J., 2006. Random forests for land cover classification. Pattern Recogn. Lett. 27, 294–300.

Goodchild, M.F., 2007. Citizens as sensors: the world of volunteered geography. GeoJournal 69 (4), 211–221.

Gosling, S.N., Bryce, E.K., Dixon, P.G., Gabriel, K.M., Gosling, E.Y., Hanes, J.M., Hondula, D.M., Liang, L., Mac Lean, P.A., Muthers, S., Nascimento, S.T., Petralli, M., Vanos, J.K., Wanka, E.R., 2014. A glossary for biometeorology. Int. J. Biometeorol. 58 (2), 277–308.

Hajat, S., Sheridan, S.C., Allen, M.J., Pascal, M., Laaidi, K., Yagouti, A., et al., 2010. Heat-health warning systems: a comparison of the predictive capacity of different approaches to identifying dangerously hot days. Am. J. Public Health 100 (6), 1137–1144.

Hattis, D., Ogneva-Himmelberger, Y., Ratick, S., 2012. The spatial variability of heat-related mortality in Massachusetts. Appl. Geogr. 33, 45–52.

Hijmans, R.J., van Etten, J., 2009. Raster. Geographic Analysis and Modeling with Raster Data: R Package Version 0.9.8-40/r681 See http://www.R-Forge.R-project.org/projects/raster/.fic (essay, and social science essay).

Ho, H.C., Knudby, A., Sirovyak, P., Xu, Y., Hodul, M., Henderson, S.B., 2014. Mapping maximum urban air temperature on hot summer days. Remote Sens. Environ. 154, 38–45.

Hondula, D., Davis, R., Leisten, M., Saha, M., Veazey, L., Wegner, C., 2012. Fine-scale spatial variability of heat-related mortality in Philadelphia County, USA, from 1983 to 2008: a case-series analysis. Environ. Heal. 11, 16.

Höppe, P., 1999. The physiological equivalent temperature — a universal index for the biometeorological assessment of the thermal environment. Int. J. Biometeorol. 43 (2), 71–75.

Höppe, P., Martinac, I., 1998. Indoor climate and air quality. Int. J. Biometeorol. 42 (1), 1–7.

Huang, W., Kan, H., Kovats, S., 2010. The impact of the 2003 heat wave on mortality in Shanghai, China. Sci. Total Environ. 408 (11), 2418–2420.

Hulley, G.C., Hook, S.J., 2009. The North American ASTER Land Surface Emissivity Database (NAALSED) version 2.0. Remote Sens. Environ. 113 (9), 1967–1975.

INVS, 2004. Étude des facteurs de risqué de décès des personnes âgées résidant à domicile Durant la vague de Chaleur d'août 2003. Institut de Veille Sanitaire (Available from http://www.invs.sante.fr/publications/2004/chaleur2003_170904/rapport_canicule.pdf).

Kaiser, R., Rubin, C.H., Henderson, A.K., Wolfe, M.I., Kieszak, S., Parrott, C.L., Adcock, M., 2001. Heat-related death and mental illness during the 1999 Cincinnati heat wave. Am. J. Forensic Med. Pathol. 22 (3), 303–307.

Katsouyanni, K., Pantazopoulou, A., Touloumi, G., Tselepidaki, I., Moustris, K., Asimakopoulos, D., Poulopoulou, G., Trichopoulos, D., 1993. Evidence for interaction between air pollution and high temperature in the causation of excess mortality. Arch. Environ. Health Int. J. 48 (4), 235–242.

King, M.D., Menzel, W.P., Kaufman, Y.J., Tanré, D., Gao, B.C., Platnick, S., ... Hubanks, P.A., 2003. Cloud and aerosol properties, precipitable water, and profiles of temperature and water vapor from MODIS. IEEE Trans. Geosci. Remote Sens. 41 (2), 442–458.

Knudby, A., LeDrew, E., Brenning, A., 2010. Predictive mapping of reef fish species richness, diversity and biomass in Zanzibar using IKONOS imagery and machine-learning techniques. Remote Sens. Environ. 114 (6), 1230–1241.

Koken, P., Piver, W., Ye, F., Elixhauser, A., Olsen, L., Portier, C., 2003. Temperature, air pollution, and hospitalization for cardiovascular diseases among elderly people in Denver. Environ. Health Perspect. 111 (10), 1312–1317.

Kosatsky, T., Henderson, S.B., Pollock, S.L., 2012. Shifts in mortality during a hot weather event in Vancouver, British Columbia: rapid assessment with case-only analysis. Am. J. Public Health 102 (12), 2367–2371.

Laaidi, K., Zeghnoun, A., Dousset, B., Bretin, P., Vandentorren, S., Giraudet, E., Beaudeau, P., 2012. The impact of heat islands on mortality in Paris during the August 2003 heat wave. Environ. Health Perspect. 120 (2), 254–259.

Liaw, A., Wiener, M., 2012. Breiman and Cutler's Random Forests for Classification and Regression. R package.

Liu, J.G., Moore, J.M., 1998. Pixel block intensity modulation: adding spatial detail to TM band 6 thermal imagery. Int. J. Remote Sens. 19, 2477–2491.

Maimaitiyiming, M., Ghulam, A., Tiyip, T., Pla, F., Latorre-Carmona, P., Halik, Ü., Sawut, M., Caetano, M., 2014. Effects of green space spatial pattern on land surface temperature: implications for sustainable urban planning and climate change adaptation. ISPRS J. Photogramm. Remote Sens. 89, 59–66.

Massetti, L., Petralli, M., Brandani, G., Orlandini, S., 2014. An approach to evaluate the intra-urban thermal variability in summer using an urban indicator. Environ. Pollut. 192, 259–265.

Masterson, J., Richardson, F.A., 1979. Humidex. A method of quantifying human discomfort due to excessive heat and humidity. Environment Canada, Downsview.

Matzarakis, A., Mayer, H., Iziomon, M.G., 1999. Applications of a universal thermal index: physiological equivalent temperature. Int. J. Biometeorol. 43 (2), 76–84.

Medina- Ramón, M., Zanobetti, A., Cavanagh, D., Schwartz, J., 2006. Extreme temperatures and mortality: assessing effect modification by personal characteristics and specific cause of death in a multi-city case-only analysis. Environ. Health Perspect. 114 (9), 1131–1136.

Meyer, D., Dimitriadou, E., Hornik, K., Weingessel, A., Leisch, F., 2012. Misc Functions of the Department of Statistics (e1071), TU Wien. R package.

Nguyen, J.L., Schwartz, J., Dockery, D.W., 2014. The relationship between indoor and outdoor temperature, apparent temperature, relative humidity, and absolute humidity. Indoor Air 24 (1), 103–112.

Nichol, J.E., To, P.H., 2012. Temporal characteristics of thermal satellite images for urban heat stress and heat island mapping. ISPRS J. Photogramm. Remote Sens. 74, 153–162.

Oke, T., 1976. The distinction between canopy and boundary -layer urban heat islands. Atmosphere 14 (4), 268–277.

Oke, T., 1988. The urban energy balance. Prog. Phys. Geogr. 12, 471–508.

Oke, T., Hay, J., 1994. The climate of Vancouver. 2nd edition B.C. Geographical Series 50. University of British Columbia, Vancouver.

Pengelly, I.D., Campbell, M.E., Cheng, C.S., Fu, C., Gingrich, S.E., Macfarlane, R., 2007. Anatomy of heat waves and mortality in Toronto. Rev. Can. Santé Publ. 98 (5), 364–368.

Prihodko, L., Goward, S.N., 1997. Estimation of air temperature from remotely sensed surface observations. Remote Sens. Environ. 60 (3), 335–346.

R Core Development Team, 2008. R: A Language and Environment for Statistical Computing Available from: http://www.R-project.org.

Rajasekar, U., Weng, Q., 2009. Urban heat island monitoring and analysis using a non-parametric model: a case study of Indianapolis. ISPRS J. Photogramm. Remote Sens. 64 (1), 86–96.

Runnalls, K., Oke, T., 2000. Dynamics and controls of the near-surface heat island of Vancouver, British Columbia. Phys. Geogr. 21 (4), 283–304.

Schifano, P., Cappai, G., De Sario, M., Michelozzi, P., Marino, C., Bargagli, A.M., Perucci, C.A., 2009. Susceptibility to heat wave-related mortality: a follow-up study of a cohort of elderly in Rome. Environ. Heal. 8, 50.

Schwartz, J., Samet, J.M., Patz, J.A., 2004. Hospital admissions for heart disease: the effects of temperature and humidity. Epidemiology 15 (6), 755–761.

Semenza, J.C., Rubin, C.H., Falter, K.H., Selanikio, J.D., Flanders, W.D., Howe, H.L., Wilhelm, J.L., 1996. Heat-related deaths during the July 1995 heat wave in Chicago. N. Engl. J. Med. 335, 84–90.

Sieber, R., 2006. Public participation geographic information systems: a literature review and framework. Ann. Assoc. Am. Geogr. 96 (3), 491–507.

Smargiassi, A., Goldberg, M.S., Plante, C., Fournier, M., Baudouin, Y., Kosatsky, T., 2009. Variation of daily warm season mortality as a function of micro-urban heat islands. J. Epidemiol. Community Health 63 (8), 659–664.

Statistics Canada. (2007). Greater Vancouver, British Columbia (Code5915) (table). 2006 Community Profiles. 2006 Census. Statistics Canada Catalogue no. 92–591-XWE. Ottawa. Released March 13, 2007.

Steadman, R.G., 1979. The assessment of sultriness. Part I. A temperature-humidity index based on human physiology and clothing science. J. Appl. Meteorol. 18, 861–873.

Stewart, I.D., Oke, T.R., 2012. Local climate zones for urban temperature studies. Bull. Am. Meteorol. Soc. 93, 1879–1900.

Strobl, C., Malley, J., Tutz, G., 2009. An introduction to recursive partitioning: rational, application, and characteristics of classification and regression trees, bagging, and random forests. Psychol. Methods 14 (4), 323–348.

Stumpf, A., Kerle, N., 2011. Object-oriented mapping of landslides using random forests. Remote Sens. Environ. 115, 2564–2577.

Su, J., Brauer, M., Buzzelli, M., 2008. Estimating urban morphometry at the neighborhood scale for improvement in modeling long-term average air pollution concentrations. Atmos. Environ. 42, 7884–7893.

Taylor, C. G. (1998). A Review of the BC Vegetation Resources Inventory Sampling Design and the Proposed Estimators. Doctoral dissertation, Simon Fraser University. Available from: https://www.stat.sfu.ca/content/dam/sfu/stat/alumnitheses/MiscellaniousTheses/Taylor.pdf.

Timm, B., McGraigal, K., 2012. Fine-scale remotely-sensed cover mapping of coastal dune and salt marsh ecosystems at Cape Cod National Seashore using Random Forests. Remote Sens. Environ. 127, 106–117.

Tomlinson, C., Chapman, L., Thornes, J., Baker, C., 2011. Including the urban heat island in spatial heat health risk assessment strategies: a case study for Birmingham, UK. Int. J. Health Geogr. 10, 42.

Trenberth, K.E., Fasullo, J.T., 2012. Climate extremes and climate change: the Russian heat wave and other climate extremes of 2010. J. Geophys. Res. Atmos. 117, D17103.

Vancutsem, C., Ceccato, P., Dinku, T., Connor, S.J., 2010. Evaluation of MODIS land surface temperature data to estimate air temperature in different ecosystems over Africa. Remote Sens. Environ. 114 (2), 449–465.

Weng, Q., Lu, D., Schubring, J., 2004. Estimation of land surface temperature - vegetation abundance relationship for urban heat island studies. Remote Sens. Environ. 89, 467–483.

Willmott, C.J., Matsuura, K., 2005. Advantages of the mean absolute error (MAE) over the root mean square error (RMSE) in assessing average model performance. Clim. Res. 30, 79–82.

WMO, 2008. Guide to Meteorological Instruments and Methods of Observation. Secretariat of the World Meteorological Organization, Geneva (681 pp. Available from https://www.wmo.int/pages/prog/gcos/documents/gruanmanuals/CIMO/CIMO_Guide-7th_Edition-2008.pdf).

Wong, M., Nichol, J., Ng, E., 2011. A study of the "wall effect" caused by proliferation of high-rise buildings using GIS techniques. Landsc. Urban Plan. 102, 245–253.

Wong, M.S., Jin, X., Liu, Z., Nichol, J., Chan, P.W., 2014. Multi-sensors study of precipitable water vapour over mainland China. Int. J. Climatol. 35, 3146–3159.
Wu, C.D., Lung, S.C.C., Jan, J.F., 2013. Development of a 3-D urbanization index using digital terrain models for surface urban heat island effects. ISPRS J. Photogramm. Remote Sens. 81, 1–11.
Xu, Y., Knudby, A., Ho, H.C., 2014. Estimating daily maximum air temperature from MODIS in British Columbia, Canada. Int. J. Remote Sens. 35 (24), 8108–8121.
Yang, J., Wong, M.S., Menenti, M., Nichol, J., 2015. Modeling the effective emissivity of the urban canopy using sky view factor. ISPRS J. Photogramm. Remote Sens. 105, 211–219.
Zakšek, K., Oštir, K., 2012. Downscaling land surface temperature for urban heat island diurnal cycle analysis. Remote Sens. Environ. 117, 114–124.
Zakšek, K., Schroedter-Homscheidt, M., 2009. Parameterization of air temperature in high temporal and spatial resolution from a combination of the SEVIRI and MODIS instruments. ISPRS J. Photogramm. Remote Sens. 64, 414–421.
Zhang, P., 1993. Model selection via multifold cross validation. Ann. Stat. 21 (1), 299–313.
Zhang, K., Li, Y., Schwartz, J., O'Neill, M., 2014. What weather variables are important in predicting heat-related mortality? A new application of statistical learning methods. Environ. Res. 132, 350–359.
Zhou, Y., Weng, Q., Gurney, K.R., Shuai, Y., Hu, X., 2012. Estimation of the relationship between remotely sensed anthropogenic heat discharge and building energy use. ISPRS J. Photogramm. Remote Sens. 67, 65–72.